DETECTION OF PLANT WATER STRESS USING UAV THERMAL IMAGES FOR PRECISION FARMING APPLICATION

AWAIS, M. – LI, W.* – YANG, Y. F. – JI, L. L.

Research Center of Fluid Machinery Engineering & Technology, Jiangsu University, China

**Corresponding author*
e-mail: lwjiangda@ujs.edu.cn; phone: +86-186-5285-0503

(Received 18th Jan 2020; accepted 24th Mar 2020)

Abstract. Adequate and real-time monitoring of water stress is critical to enhance productivity, crop quality, as well as water use efficiency. This study contributes to the new approach of precise and rapid estimation of real-time water stress using thermal images taken with an Unmanned aerial vehicle. Different physiological parameters stomatal conductance (gs), leaf area, and ground reality parameter (Tc) were calculated between 11.30 and 13.30 (Chinese standard time) on sampling day. The volumetric water content (θ, m^3 m^{-3}) of the soil at different depths of (20, 40, and 60 cm) was measured. Data processing steps were implemented in MATLAB for thermal images to calculate the canopy temperature T_1. Empirical (CWSIe) and statistical (CWSIs) methods of CWSI were applied for model calibration. Results showed that different spectral indices (TCARI, NDVI, OSAVI TCARI/OSAVI) had a high correlation with stomatal conductance (gs) ($R^2 = 0.590$) and transpiration rate (tr) ($R^2 = 0.602$) as compared to CWSIe and CWSIs. Volumetric water content (θ) and CWSIsi have a high correlation coefficient (0.872). However, the transpiration rate shows a week correlation with spectral indices (TCARI, NDVI, OSAVI, and TCARI/OSAVI) as compared with CWSI. The plotted high- resolution map shows the distribution of water stress in different irrigation treatments and potentially applied in precision irrigation management.
Keywords: *stomatal conductance, precision agriculture, PIX4D software, unmanned aerial vehicles, remote sensing*

Introduction

Uses of water in sustainable agriculture has become a precarious issue in all developing countries, because of climate and water scarcity changes, so accurate irrigation water management strategies are required. In general terms, agriculture consumes most of the world water resources (Jiang et al., 2013). At the same time, other industries are trying to consume more and more water, and thus people are competing with food production. Globally 46% of the food supply is produced from the agricultural land, which covers only 18% of the cultivated land (Döll and Siebert, 2002). So, it is essential to manage irrigation with the optimal use of water. Worldwide, farmers are facing many problems, particularly in semi-arid areas, related to agriculture water resources (Gonzalez-Dugo et al., 2010; Jin et al., 2018). Plant transpiration and climate change affect the crop productivity, quality and soil water balance significantly.

Using thermal information for identifying plant water stress at ground level with thermal sensors become popular in the 1960s (Tanner, 1963). Crop water stress index (CWSI) has been familiarized for indicating water stress of crop based on the difference between air temperature and greenery of the crop (Jackson et al., 1981; Jones, 2013; Idso et al., 1981) which is most commonly used as the indicator of plant water status derived from canopy temperature. Jones (1999) developed a new reformulated CWSI by the difference between threshold temperature and canopy temperature (T_{Canopy}), which is normalized by the difference in temperature between T_{wet} (full transpiring temperature)

http://www.aloki.hu ● ISSN 1589 1623 (Print) ● ISSN 1785 0037 (Online)
DOI: http://dx.doi.org/10.15666/aeer/1803_40874102

and T_{dry} (non-transpiring temperature) as upper and lower reference temperature (Jones, 1999). In order to calculate crop water stress index (CWSI) (Jackson et al., 1981) proposed a method to calculate the theoretical CWSI with the theory of crop energy balance, but this approach needs too many metrological data. For obtaining the design parameter of empirical CWSIe, the secure method is to analyze the normalized temperature of the canopy (Jones, 1999; Jones et al., 2002) over calculating wet reference (T_{wet}) temperature and dry reference (T_{dry}) temperature. However, the location of reference leaf and metrological factors are easily distributed; these essential reference surfaces and CWSI may not be the same in a different region. Another feasible method for calculating (T_{wet}) from the temperature histogram of the average of the lowest 5% and (T_{dry}) temperature is supposed to be the same as (T_{air}) air temperature +50 °C (Cohen et al., 2005, 2017; Rud et al., 2014; Agam et al., 2014). In the agricultural sector, one of the most generally oppressed in remote sensing is optical or visual (RS) remote sensing. It uses different bands, i.e., SWIR (short wave infrared) and NIR (near-infrared) sensors, to get pictures from ground surfaces by reflecting phenomena from the target area surface (Prasad and Bruce, 2011). Satellite images are collected by using visible, NIR, traditional aircraft and Unmanned Aerial Vehicles (UAVs). Numerous studies (Hatfield and Prueger, 2010; Jordan, 1969) have monitored crop conditions in the agriculture sector.

In contrast, thermal sensors were used to detect surface temperature, and it was found to be a very quick response variable for monitoring crop health and crop stress (Anderson et al., 2013; Stark et al., 2014). Thermal remote sensing is a process that measures the radiation that is discharged from a surface body and transforming into temperature values without producing any interaction with an object. All surface object emits radiation with a temperature above 0 K or -273 °C (Khanal et al., 2017). The intensity of radiation of each object depends on the temperature, the higher the temperature the greater the intensity of the radiation is. Thermal remote sensing provides us with significant fluxes of temperature and energy from the earth's surface which are necessary to converse the landscape's processes and responses (Quattrochi and Luvall, 1999; De-Cai et al., 2012).

CWSI estimation with TIR imagery is a practical approach that was introduced to eliminate the VIS imagery with the co-registration method (Meron et al., 2010). Many studies on assessing CWSI approaches through remote sensing have concentrated on image processing techniques from the nearby ground platform, to detect the stress level at different crop levels (Möller et al., 2006). Statically modeling techniques were used to calculate the lower reference temperature and canopy related temperature in TIR imagery. Recently detection of water stress from (UAVs) has been used worldwide with a higher spatial resolution with a potential of providing new ideas for farmers to observe the water stress at field level (Berni et al., 2009; Poblete-Echeverría et al., 2014; Espinoza et al., 2017). It is necessary to develop a new approach for measuring CWSI by using temperature histogram from UAV thermal Images and analyze water stress of crop and improve the irrigation efficiency. Overall objectives of this research are to (1) exclude soil background pixels to get the pure canopy pixel using different edge detection method and series of UAV thermal imagery: (2) estimate the values of (T_{wet}), (T_{dry}) and (T_{canopy}) from the histogram of canopy temperature which is simply recognized from UAV thermal images; (3) determine and optimize correlation to successfully identify the water stress from field condition by comparing different parameters of CWSI and spectral indices.

http://www.aloki.hu ● ISSN 1589 1623 (Print) ● ISSN 1785 0037 (Online)
DOI: http://dx.doi.org/10.15666/aeer/1803_40874102

Materials and methods

Experimental design

This study was conducted in a cultivated land of 1.13-ha research field in a tea garden located at the (right) bank of the Yangtze River in Jiangsu Province, PR China (32°1′00″N, 119°4′00″E), with an elevation of 18.5 m above sea level. The tea plant was four-year-old Anji white tea, with a plant row spacing of 1.5 m and plant spacing with the row of 1 m. This research field was divided and completely randomized with four irrigation treatments with three replicates. Site area soil is silty-loam texture. The climate in this area is semi-arid, and the annual rainfall and ET_0 respectively are 360 mm and 1094 mm, for the year 2019. There were four randomized irrigation treatments with three replications and a total of 12 experimental plots, and each plot was designed to be 4 m wide (7 rows) and 5 m long. The four treatments were (T_4) severe water stress, (T_3) moderate water stress, (T_2) mild water stress, and (T_1) full irrigation. These twelve plots were selected randomly, and different treatment was irrigated to keep up the volumetric water content on a different level of the field capacity, respectively. In order to maintain the difference in irrigation, the four treatment plots were watered to maintain the volumetric soil water content at 90-100%, 75%, 60%, and 50% of the field capacity, respectively. Drip irrigation controller system was installed to irrigate the land, and an individual solenoid valve was opened and closed, which corresponding to each irrigation sector with one line per row had a stream rate of 1.5 Lh^{-1} and were spaced 0.85 m apart. In each plot, three sites for data gathering were selected for ground truth data. For post-processing image calibration, Pix-4D mapper was used in this research for obtaining thermal infrared mosaic images (*Fig. 1*). FLIR Tools software was also used for temperature calibration parameters, i.e., relative humidity, target distance, background temperature, and emissivity.

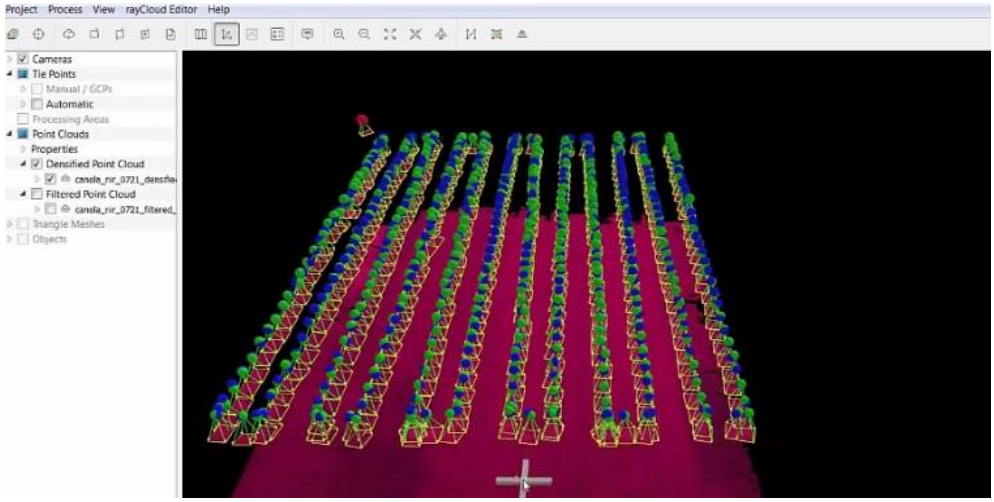

Figure 1. *Post-processing calibration in Pix4d software*

Aerial image acquisition and software solutions

Figure 2 shows the main procedure of acquisition and pre-treatment of UAV imageries. A multi-rotor UAV drone manufactured by DJI (S900) equipped with RGB and thermal cameras (Zenmuse XT, FLIR System, Inc., USA) was used to measure the

http://www.aloki.hu ● ISSN 1589 1623 (Print) ● ISSN 1785 0037 (Online)
DOI: http://dx.doi.org/10.15666/aeer/1803_40874102

canopy temperature. Temperature and spectral range of thermal cameras are 7.5-13 µm, with a resolution of 640 × 512 pixels, thermal sensitivity < 0.05 °C at + 30 °C and focal length of 25 mm. Due to its high matrices and multi-rotor function, they have a capability for a stable and safe flight with a long battery. The flying speed of UAV is 2.5 ms^{-1} with a high elevation of 80 m beyond the earth's surface with a sample space distance of 6.12 cm and has sufficient overlap for photogrammetric processing. The most significant uncertainty occurring in thermal mapping is sensor calibration. In our case, there is automatic sensor calibration while obtaining thermos MAP. Evaposensors (Skye Instruments, Llandrindod Wells, UK) were used to acquire the canopy reference temperature indices T_{wet} and T_{dry} for supporting the segmentation of the thermal image.

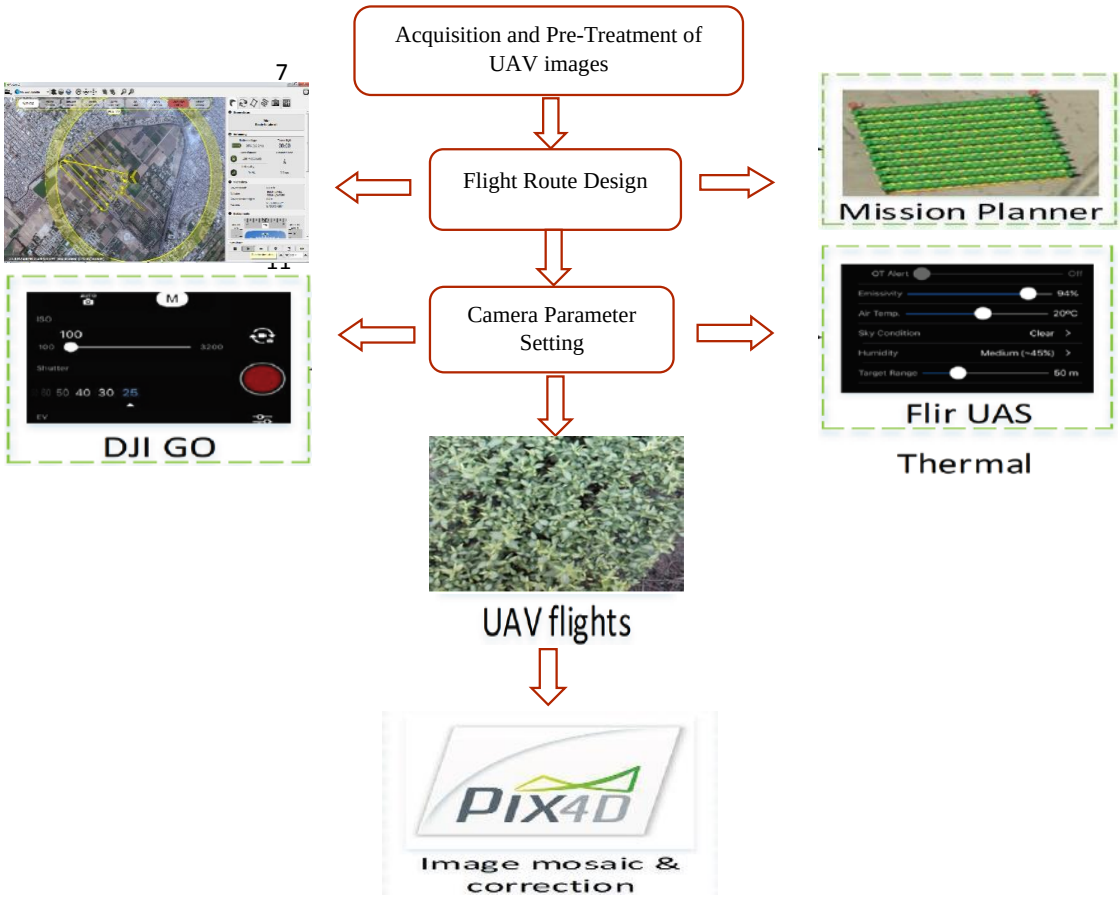

Figure 2. *Flow chart of image acquisition and pre-treatment of an unmanned aerial vehicle*

Physiological data collection

Leaves temperature for thermal image calibration was calculated regarding five sunny leaves and five sheltered leaves using a portable infrared thermometer (TN410LCE, ZyTemp, Radiant Innovation Inc.) at the same time with UAV image acquisition. Different physiological parameter stomata conductance (Ahrenfeldt et al., 2013), ground truth Tc, soil water content, and leaf area was calculated around 11.30 and 13.30 (Chinese standard time) on sampling day. Transpiration rate (tr, $mmolm^{-2}\ s^{-1}$) and the stomatal conductance (gs, mol $m^{-2}\ s^{-1}$) of the leaves were calculated using a portable photosynthesis system (LI-6400, LI-COR Inc. USA). The leaf was the fourth

http://www.aloki.hu ● ISSN 1589 1623 (Print) ● ISSN 1785 0037 (Online)
DOI: http://dx.doi.org/10.15666/aeer/1803_40874102

from the upper part of the tea canopy and fully exposed to the sun, and three leaves per plot were measured. LAI was measured 2 h earlier before sunset just to avoid the effect of direct sunlight. The 'soil volumetric' water content (θ, $m^3 m^{-3}$) at different depths (20, 40, and 60 cm) was measured using soil moisture sensors (Decagon EM50 data logger, ECH20 sensor), when thermal infrared images were collected. Ground-truth Tc was measured by a handheld infrared thermometer (RAYTEK, ST60+, Raytek Inc., Santa Cruz, USA) with a temperature range of 32-600 °C and a spectral range of 8-12 μm.

Data processing

Data processing steps were implemented in MATLAB R2016b (Math works Inc., Matick, MA, USA) for thermal images to calculate the T_1. Mapping of CWSI and extraction of canopy pixels from soil and other non-leaf material must be required. Calculation of T_1 must require transparent canopy pixel from thermal images to show the higher temperature during midday periods. Edge recognition methods were used to exclude soil background pixels to get the transparent canopy pixel using Matlab. These edge detection methods are designed in the vertical and horizontal direction to identify gradient changes extremely to boundaries (Maini and Aggarwal, 2008). In this stage, two other edge detection methods Roberts and Prewitt, can also be applied to check the changes in gradient and edges of images. The mixed pixel was intensified for more conservative elimination, which is further dispersed up to more six pixels along and across the edge direction of the thermal gradient.

CWSI calculation

This study was suggested by (Jones, 2013) to estimate the CWSI algorithm, which can be represented as follows:

$$CWSI = \frac{K_{Conopy} - T_{Wet}}{K_{Dry} - T_{Wet}} \quad \text{(Eq.1)}$$

where T_{canopy} is the temperature that is acquired by aerial TIR images, T_{wet} is the lower reference temperature or entirely transparence leaf, and T_{dry} is the non-transpiring leaf temperature, which is also called an upper reference. The CWSI was acquired using simplified, statistical, and empirical approaches based on T_{dry} and T_{wet} values. The temperature of fully transpiring plants leaves was measured using a spray of water on both sides of leaf (T_{wet}), and petroleum jelly was used to calculate the temperature of non-transpiring leaves covered with jelly (T_{dry}). In this approach, individually, numerical analysis is performed to measure the threshold values of T_{wet} and $T_{dry,}$ which is dependent on sub-regions. Initially, TIR images were used to generate the temperature histogram for each region. Different studies assume that T_{wet} from the histogram is derived from the coldest part, and further, T_{dry} is derived from the highest part of the histogram (Rud et al., 2014). Different spectral indices were also calculated using spectral reflectance of the canopy, i.e., transformed chlorophyll absorption for reflectance index (TCARI), Normalize Difference Vegetation Index (NDVI), optimize soil adjusted vegetation index (OSAVI).

$$TCARI = 3 * \left[\left(R700 - R670\right) - 0.2 * \left(R700 - R55O\right) * \left(R700 / R670\right)\right] \quad \text{(Eq.2)}$$

http://www.aloki.hu ● ISSN 1589 1623 (Print) ● ISSN 1785 0037 (Online)
DOI: http://dx.doi.org/10.15666/aeer/1803_40874102

$$OSAVI = (1 + 0.16) * (R800 - R670) / (R800 + R670 + 0.16) \quad \text{(Eq.3)}$$

$$NDVI = \frac{R800 - R680}{R800 + R680} \quad \text{(Eq.4)}$$

Adaptive T_{wet} and T_{dry}

A static approach is proposed to estimate the threshold values of $T_{wet,}$ and T_{dry} which depends on the regions. The histogram temperature was acquired as shown in the flow chart (*Fig. 3*). The average density distribution and distinctive bimodal are the histogram feature which is used to represent the soil pixels and vegetated pixels. In this study, Gaussian mixture modeling (GMM) was used to estimate the typical values of T_{wet} and T_{dry} for canopy by fitting temperature distribution to cluster soil/canopy pixel. In the Gaussian distribution component, higher temperature representing the non-canopy pixel of soil background affects Gaussian distribution.

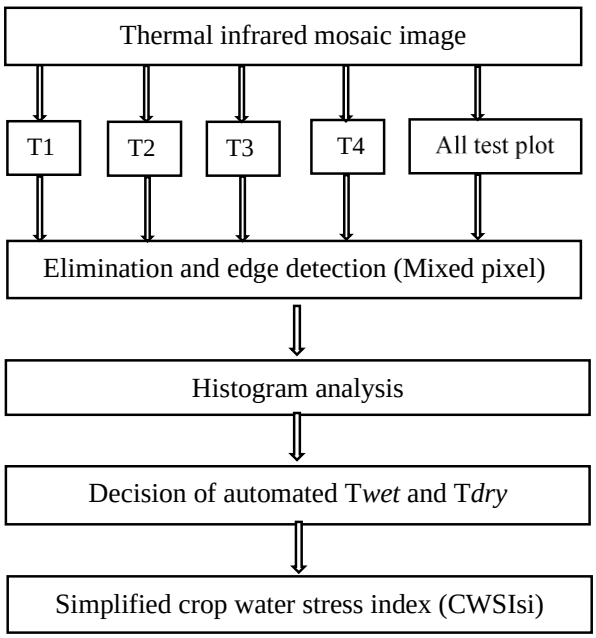

Figure 3. *Flow chart of detection (CWSI) using temperature histogram approach*

Results

Feature extraction

CWSI mapping required feature extraction of canopy pixel from the soil background images, which must have excluded non-leaf material and soil from the UAV images. Different canopy edge detection was used to show the transparent canopy pixel of higher temperature during midday of periods and compared these methods to indicate the raster image between copy and soil background pixel. *Figure 4* shows a vibrant edge detection of the canopy plant by using edge detection algorithm in the raster image, and the mixture of crop canopy and pixel of different edges were screened out from orthomosaic images. White pixels show the temperature of clear canopy that was acquired.

http://www.aloki.hu ● ISSN 1589 1623 (Print) ● ISSN 1785 0037 (Online)
DOI: http://dx.doi.org/10.15666/aeer/1803_40874102

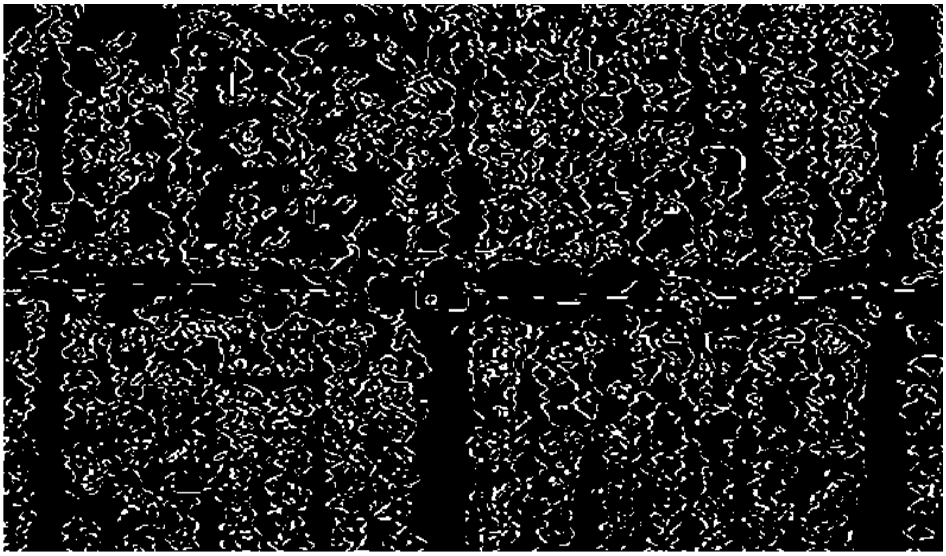

Figure 4. *Example of the orthomosaic image with Edge detection methods*

Canopy temperature histogram and calculation of CWSI

Images from UAV thermal cameras were used to obtain the canopy temperature histogram based on the irrigation treatment of entire experiment plants. T_{wet} and T_{dry} values were attained from the average of the highest and the lowest values of 0.5% from canopy temperature histogram, respectively. *Figure 5* shows the surface temperature distribution of soil and canopy pixels from each experimental plot, which was bimodal (*Fig. 5a*). This soil and canopy temperature histogram represent the mixture of bare and dry soil, whereas it shows transpiring and actively growing canopies. This histogram's bimodal distribution featured representing soil and vegetation background in between 23 and 43 °C due to the difference of apparent temperature up to 34 °C. To remove the accuracy of CWSI, removal of soil background is very crucial, so after soil background was removed, the temperature distribution was Gaussian (*Fig. 5b*).

T_{wet} values of different methods for CWSI was 25.8 °C, 28.9 °C, and 28.5 °C. Canopy and soil background temperature for selected plots are shown in *Figure 5*. Therefore, experimental results of temperature histogram stated that the temperature of canopy pixel is worse than that of soil pixel. The air temperature was measured from the entire experiment plots, and it was 38.3 °C. From this temperature, a considerable gap difference shows, which represents the undefined error in the measured values of T_{wet} and T_{air}. So T_{wet} values of CWSIs and simplified CWSI (CWSIsi) methods were approximately similar. Furthermore, the T_{dry} values of CWSIsi, CWSIs, and CWSIe were 39.4 °C, 43.8 °C, and 44.2 °C. Ti values of four different irrigation treatment plants were derived and analyzed the apparent difference from canopy temperature histogram. Soil and canopy temperature distribution of these four different treatments are shown in *Figure 6*. Results showed that plot 4 (T_4) has the highest temperature value of T_i (35.6 °C) than T_2, T_3, and T_1. These four treatments plot show higher difference among the values of T_i that is obtained from the histogram approach, so canopy edged detection approach is an acceptable method to calculate the canopy temperature.

http://www.aloki.hu ● ISSN 1589 1623 (Print) ● ISSN 1785 0037 (Online)
DOI: http://dx.doi.org/10.15666/aeer/1803_40874102

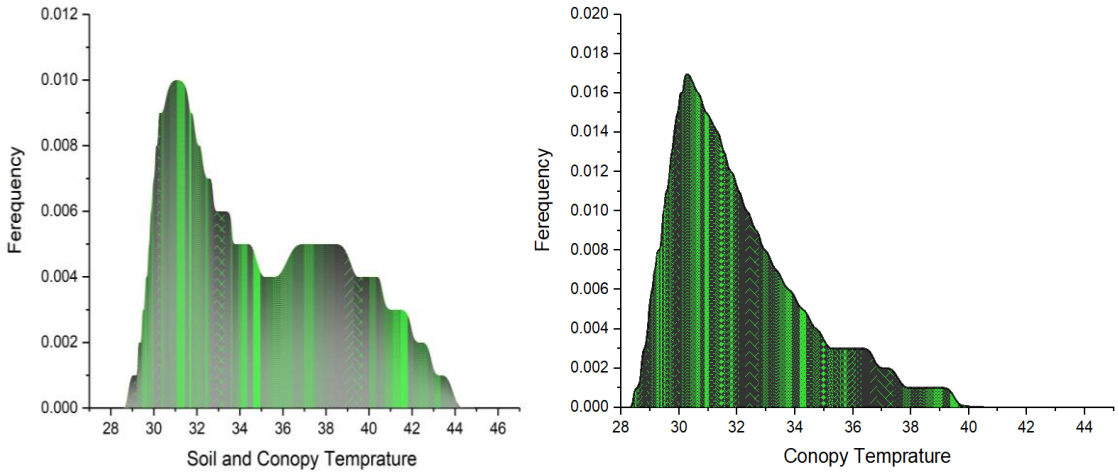

a b

Figure 5. *Histogram (canopy and soil pixels) of temperatures of the entire experimental plot (a), Histogram (canopy pixels) of canopy temperatures of the entire experimental plot (b). Note: dark black lines of histogram represent null temperature values*

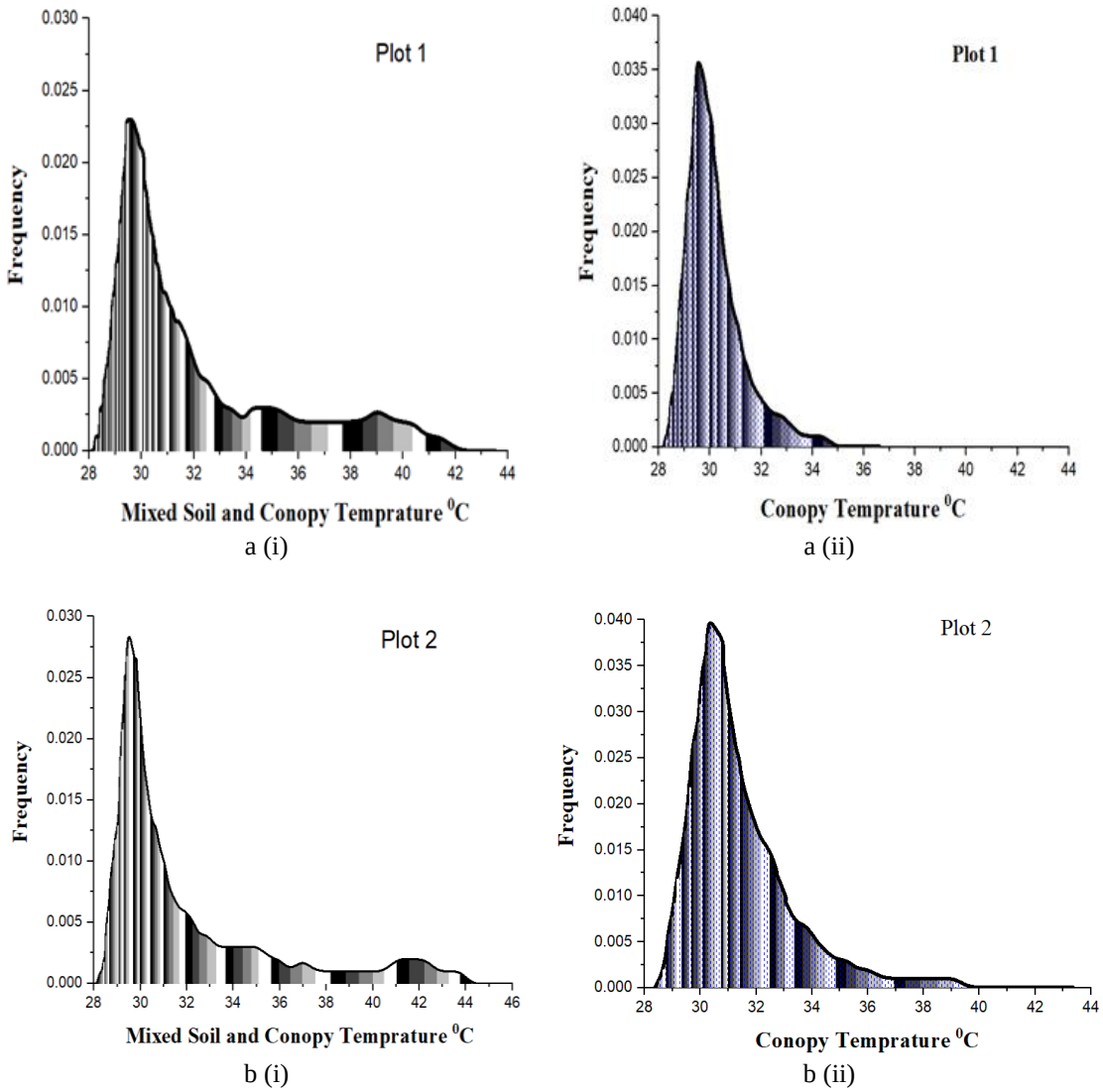

a (i) a (ii)

b (i) b (ii)

http://www.aloki.hu ● ISSN 1589 1623 (Print) ● ISSN 1785 0037 (Online)
DOI: http://dx.doi.org/10.15666/aeer/1803_40874102

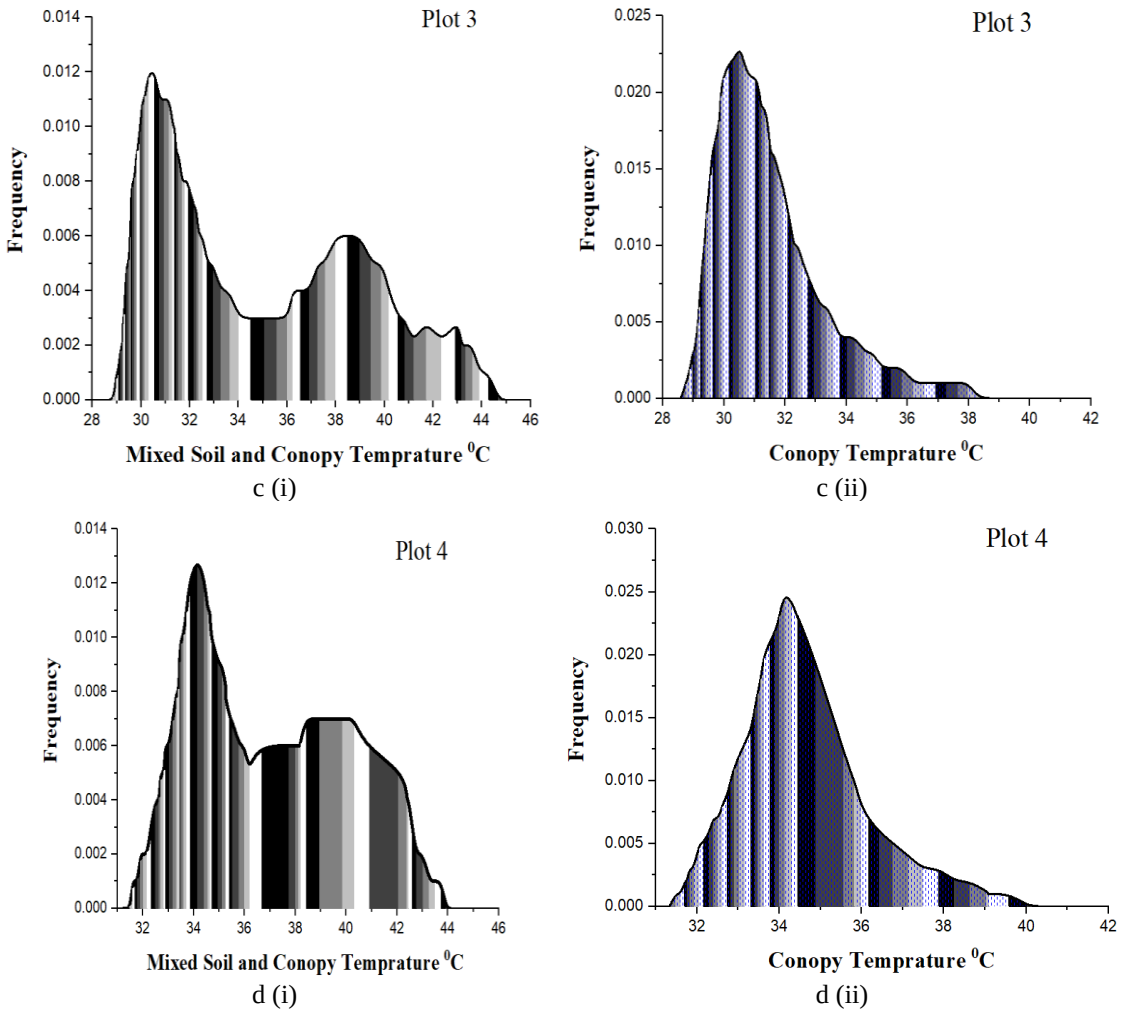

Figure 6. *Temperature histograms of soil pixel and canopy pixels for each experimental plot (a–d). (i) Mixed canopy and soil pixels, ii canopy pixel*

Relationship of CWSI and physiological indicators

Many researchers (Gago et al., 2013; Jones, 1999; Pallavi et al., 2017) have proved that values of CWSI and stomatal conductance have a high correlation. *Figure 7* shows the relationship of stomatal conductance with different CWSI values from the UAV thermal camera images. Stomatal and transpiration rates were calculated to identify the accurateness of CWSI by different parameters. Results revealed that stomatal conductance (gs) shows a negative correlation with three different models of calculating CWSI, and the value of R^2 (coefficient of determination) is different.

While taking thermal images on the same day transpiration rate was also considered at midday. The result stated that (*Fig. 8*) there is a negative correlation between transpiration rate and simplified, statistical, and experimental values with CWSI and R^2 values remained 0.519, 0.501, and 0.5696 individually. CWSI from the histogram approach highly correlated with the measured transpiration rate, which reflects the water stress of crop (*Fig. 8a-c*). Experimental results suggest that water stress from the histogram approach is highly accepted and accurately shows the water stress condition. Besides, it can be observed (*Fig. 8d-g*) that transpiration rate has a

http://www.aloki.hu ● ISSN 1589 1623 (Print) ● ISSN 1785 0037 (Online)
DOI: http://dx.doi.org/10.15666/aeer/1803_40874102

week correlation of spectral indices (TCARI, NDVI, OSAVI TCARI/OSAVI) as compared with CWSI.

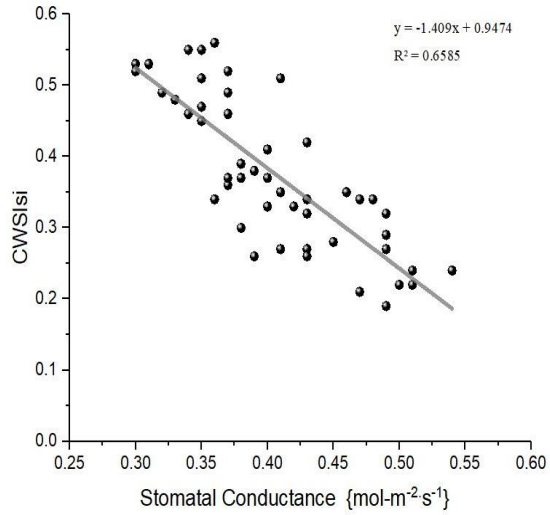

a

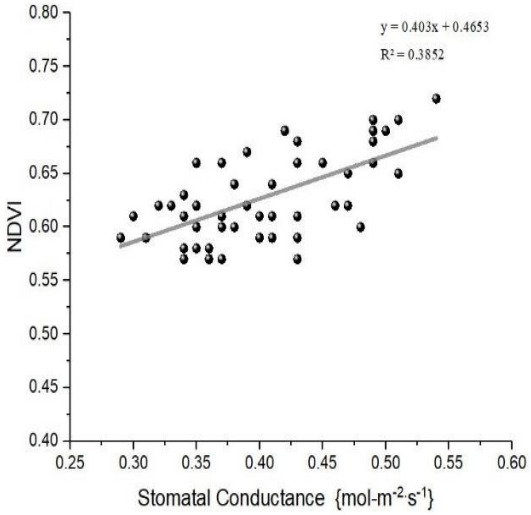

b

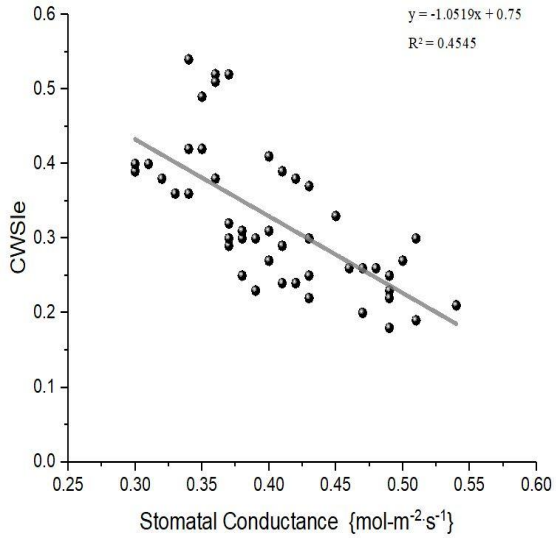

c

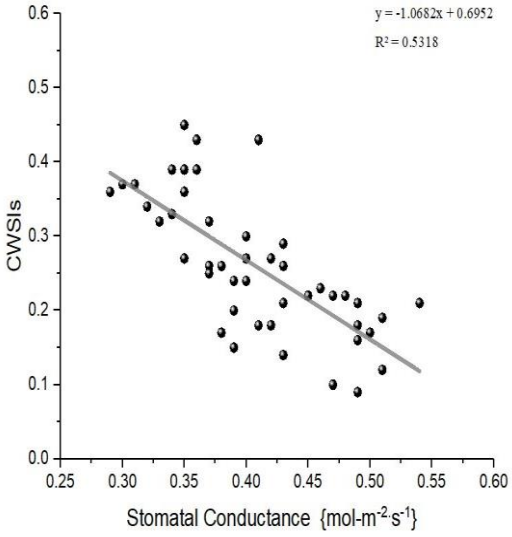

d

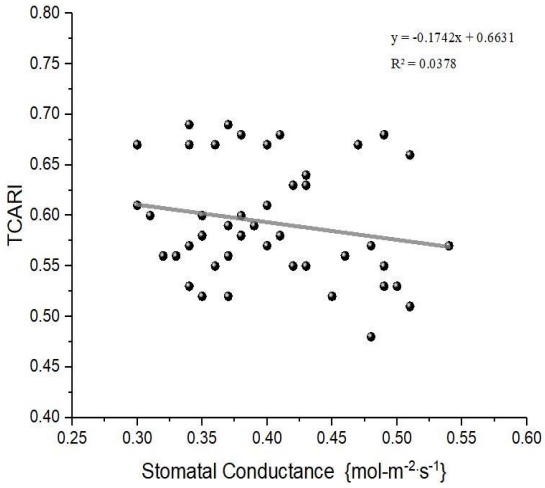

e

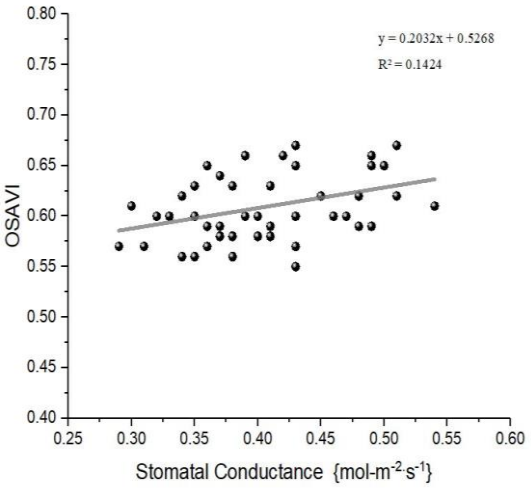

f

http://www.aloki.hu ● ISSN 1589 1623 (Print) ● ISSN 1785 0037 (Online)
DOI: http://dx.doi.org/10.15666/aeer/1803_40874102

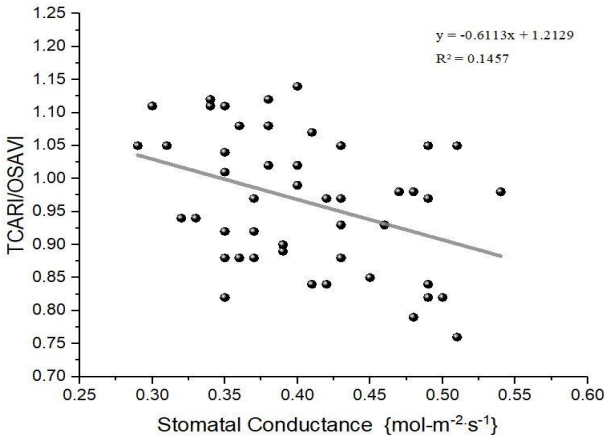

g

Figure 7. *Stomatal conductance relationship with and (a) empirical (b) statistical (c) simplified CWSI (d) (NDVI), (e) (TCARI), (f) (OSAVI), (g) TCARI/OSAVI*

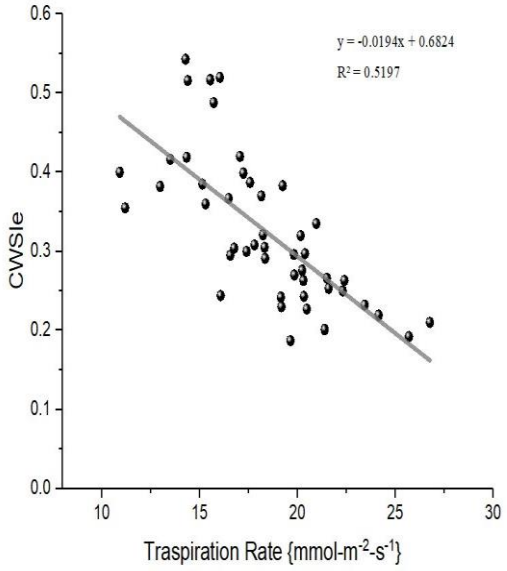

a

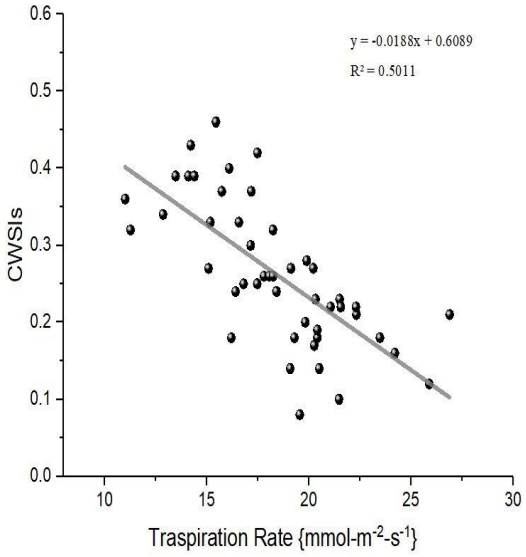

b

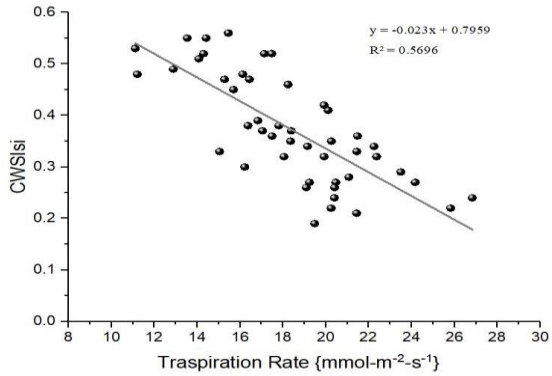

c

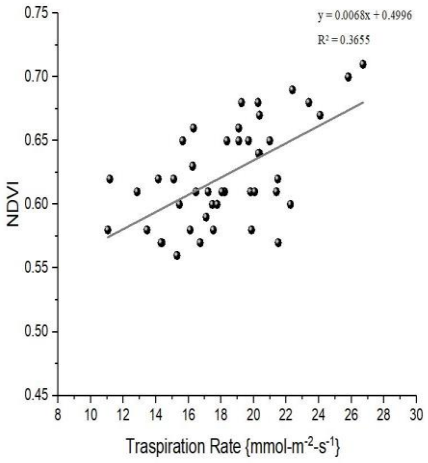

d

http://www.aloki.hu ● ISSN 1589 1623 (Print) ● ISSN 1785 0037 (Online)
DOI: http://dx.doi.org/10.15666/aeer/1803_40874102

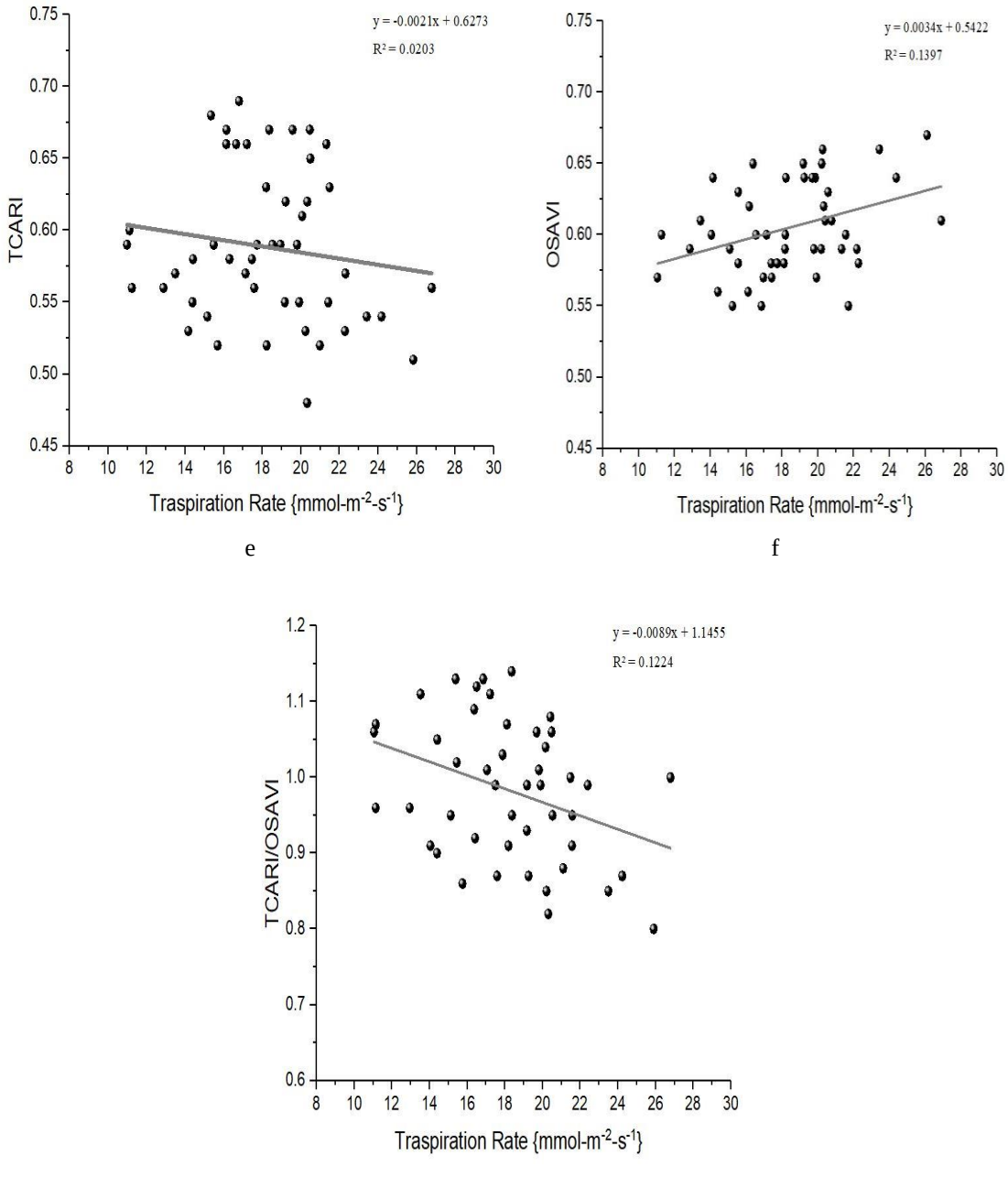

Figure 8. *Transpiration rate relationship with (a) empirical (b) statistical (c) simplified CWSI (d) (NDVI), (e) (TCARI), (f) (OSAVI), (g) TCARI/OSAVI.*

Adaptive CWSI mapping

Figure 9 shows the high-resolution predictable map of the CWSI index, which is based on the values of T_{wet} and T_{dry} in four different experimental plots for agriculture water management. Detailed values of CWSIsi of water deficit are in between 0.100 to 0.810, and the exact mean values of water stress index of four plots remained 0.161, 0.362, 0.521, and 0.692 individually. This water stress map shows a stable relationship between the water stress condition of plots and CWSIsi.

http://www.aloki.hu ● ISSN 1589 1623 (Print) ● ISSN 1785 0037 (Online)
DOI: http://dx.doi.org/10.15666/aeer/1803_40874102

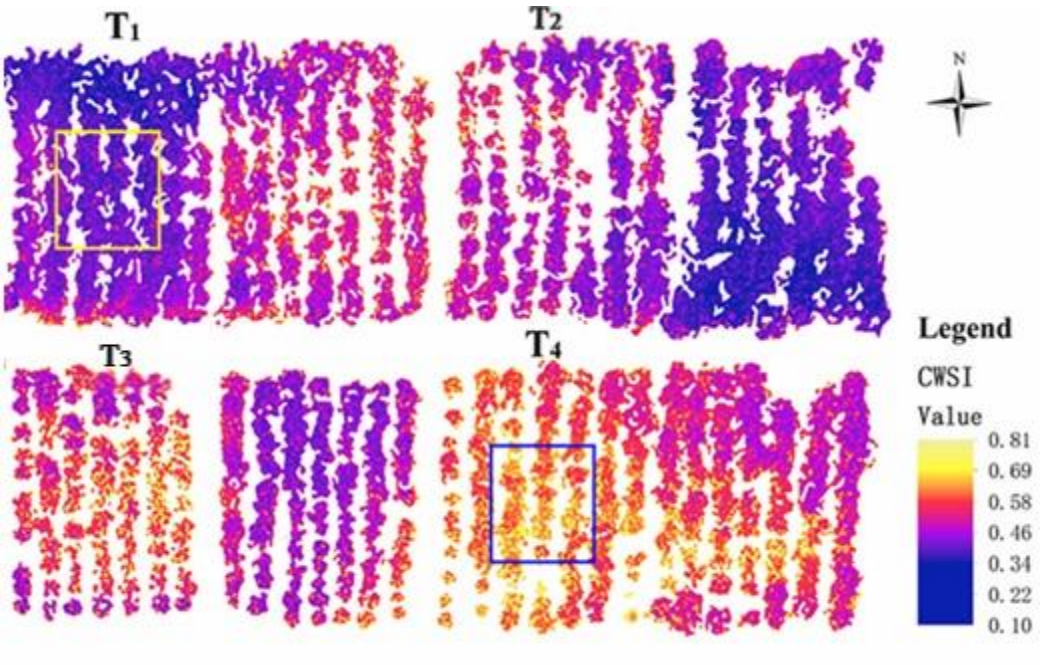

Figure 9. *Example of Adaptive CWSI mapping*

Discussion

In this study, the ability of UAV technology with thermal camera images was used to determine the crop water status at the canopy scale. However, CWSI provides a critical piece of information for irrigation water management. Furthermore, soil background pixel was eliminated to get the transparent canopy pixel using different edge detection methods, and series of UAV thermal imagery and canopy temperature histogram approach was employed to calculate the CWSIsi parameter (T1, T_{wet}, and T_{dry}). CWSI is a handy parameter for assessing the water stress condition of the crop. Many previous studies (Pallavi et al., 2017; Davcev et al., 2018) stated that there is a perfect relationship between stomatal conductance, transpiration rate, and CWSI, respectively. The proposed methods were based on the assumption that there exists a water stress level in the field for representing canopy temperature values for stress and non-stress plants, and no metrological data is essential for the calculation of CWSIsi. To calculate the CWSI from the canopy temperature, soil background pixels should be removed from the UAV thermal camera images. In this work, ArcGIS and Pix4D software were used to pre-process the UAV thermal images (*Fig. 4*). The average canopy temperature of different four plots which is carried out by edge detection algorithm is T4 (35.6 °C), T3 (31.9 °C), T2 (31.2 °C), and T1 (30.1 °C) respectively. This temperature difference results have been proved with previous research (García-Tejero et al., 2016; Testi et al., 2008). T_{dry} values can be calculated by different methods, and values of simplified, statistical, and empirical water stress was 39.4 °C, 43.8 °C, and 44.2 °C. Previous studies also suggested the reasonable values of T_{dry} temperature are 39.2 °C (Khorsandi et al., 2018). A bimodal histogram was obtained before the removal of soil background pixels, this histogram approach not only explained the temperature difference but also showed us the partially overlapping temperature.

Besides, this approach for estimating CWSI is not a direct method for the measurement of actual water stress since its mean values can fluctuate with

http://www.aloki.hu ● ISSN 1589 1623 (Print) ● ISSN 1785 0037 (Online)
DOI: http://dx.doi.org/10.15666/aeer/1803_40874102

environmental factors and moisture conditions. Crop physiological indicator and water stress induce relationship were compared and observed that values of R^2 of stomatal conductance and TCARI, NDVI, OSAVI, TCARI/OSAVI are 0.037, 0.385, 0.142, and 0.145. The R^2 value of CWSIsi calculated from the histogram approach (0.658) is higher than other CWSIs statistical (0.531) and CWSIe empirical (0.454), respectively. Some previous studies also suggested the low correlation between stomatal and these spectral indices TCARI, NDVI, OSAVI, TCARI/OSAVI (Gago et al., 2013; Baluja et al., 2012). The values of empirical and statistical water stress range from 0.14 to 0.53 and 0.04 to 0.49, while the values of simplified water stress are 0.14 to 0.55, respectively. These values are expected from the different approaches for estimated values of T_{wet} and T_{dry} temperature, which was measured from the average values of the highest and the lowest 0.5% from canopy temperature histogram approach. The temperature of fully transpiring plants leaves was measured using a spray of water on both sides of leave (T_{wet}), and petroleum jelly was used to calculate the temperature of non-transpiring leave covered with jelly (T_{dry}). Furthermore, wet and dry temperature values of simplified water stress are stable and easy to calculate. This study is carried out in one flight of UAV, and our finding suggested that CWSI may be applied for precision irrigation management.

Conclusion

This study proposed new techniques for the calculation of adaptive water stress index using a different approach: 1) canopy pixel extraction from different detection algorithm and statistical analysis approach for surface temperature distribution and histogram method is a very operational tool for the judgment of crop water stress: 2) adaptive CWSIsi and efficient determination of (wet) and (dry) references, and T_1 is the more vigorous parameter for CWSIe, CWSIs, TCARI, NDVI, OSAVI, TCARI/OSAVI. T_{wet} and T_{dry} values were attained from the average of the highest and the lowest values of 0.5% from canopy temperature histogram, respectively. A strong linear relationship between adaptive CWSIsi and stomatal conductance was obtained. The current approach exists hypothetically and provides us a practical method for plant water stress calculation with a high spatial resolution at the field scale and plant for automated irrigation purposes. As for future work, further research will consider the effects of different vintages, and various phenotypic phases will be examined and applied to these methods for the control system of highly efficient, intelligent irrigation systems.

Acknowledgments. The authors would like to acknowledge the Jiangsu University, China, for their support in providing experiment station and filed. The work was sponsored by the synergistic innovation, center of Jiangsu modern agriculture equipment, and technology (No. 4091600014).

Conflict of interests. The authors reported no potential conflict of interests.

REFERENCES

[1] Agam, N., Segal, E., Peeters, A., Levi, A., Dag, A., Yermiyahu, U., Ben-Gal, A. (2014): Spatial distribution of water status in irrigated olive orchards by thermal imaging. – Precision Agriculture 15: 346-359.

http://www.aloki.hu ● ISSN 1589 1623 (Print) ● ISSN 1785 0037 (Online)
DOI: http://dx.doi.org/10.15666/aeer/1803_40874102

[2] Ahrenfeldt, J., Egsgaard, H., Stelte, W., Thomsen, T., Henriksen, U. B. (2013): The influence of partial oxidation mechanisms on tar destruction in two-stage biomass gasification. – Fuel 112: 662-680.
[3] Anderson, M. C., Hain, C., Otkin, J., Zhan, X., Mo, K., Svoboda, M., Wardlow, B., Pimstein, A. (2013): An intercomparison of drought indicators based on thermal remote sensing and NLDAS-2 simulations with us drought monitor classifications. – Journal of Hydrometeorology 14: 1035-1056.
[4] Baluja, J., Diago, M. P., Balda, P., Zorer, R., Meggio, F., Morales, F., Tardaguila, J. (2012): Assessment of vineyard water status variability by thermal and multispectral imagery using an unmanned aerial vehicle (UAV). – Irrigation Science 30: 511-522.
[5] Berni, J., Zarco-Tejada, P., Sepulcre-Cant, G., Fereres, E., Villalobos, F. (2009): Mapping canopy conductance and CWSI in olive orchards using high resolution thermal remote sensing imagery. – Remote Sensing of Environment 113: 2380-2388.
[6] Cohen, Y., Alchanatis, V., Meron, M., Saranga, Y., Tsipris, J. (2005): Estimation of leaf water potential by thermal imagery and spatial analysis. – Journal of Experimental Botany 56: 1843-1852.
[7] Cohen, Y., Alchanatis, V., Saranga, Y., Rosenberg, O., Sela, E., Bosak, A. (2017): Mapping water status based on aerial thermal imagery: comparison of methodologies for upscaling from a single leaf to commercial fields. – Precision Agriculture 18: 801-822.
[8] Davcev, D., Mitreski, K., Trajkovic, S., Nikolovski, V., Koteli, N. (2018): IOT agriculture system based on Lorawan. – 14th IEEE International Workshop on Factory Communication Systems (WFCS), 2018, IEEE 1-4.
[9] De-Cai, W., Zhang, G.-L., Xian-Zhang, P., Yu-Guo, Z., Ming-Song, Z., Gai-Fen, W. (2012): Mapping soil texture of a plain area using fuzzy-c-means clustering method based on land surface diurnal temperature difference. – Pedosphere 22: 394-403.
[10] Döll, P., Siebert, S. (2002): Global modeling of irrigation water requirements. – Water Resources Research 38: 8-1-8-10.
[11] Espinoza, C. Z., Khot, L. R., Sankaran, S., Jacoby, P. W. (2017): High resolution multispectral and thermal remote sensing-based water stress assessment in subsurface irrigated grapevines. – Remote Sensing 9: 961.
[12] Gago, J., Martorell, S., Tom, S. M., Pou, A., Mill, N. B., Ram. N. J., Ruiz, M. S., Nchez, R., Galm, S. J., Conesa, M. (2013): High-resolution aerial thermal imagery for plant water status assessment in vineyards using a multicopter-RPAS. – First Conference of the International Society for Atmospheric Research Using Remotely-Piloted Aircraft, Palma de Mallorca, Spain.
[13] Garc A-Tejero, I., Costa, J., Egipto, R., Dur N-Zuazo, V., Lima, R., Lopes, C., Chaves, M. (2016): Thermal data to monitor crop-water status in irrigated Mediterranean viticulture. – Agricultural Water Management 176: 80-90.
[14] Gonzalez-Dugo, V., Durand, J.-L., Gastal, F. (2010): Water deficit and nitrogen nutrition of crops. A review. – Agronomy for Sustainable Development 30: 529-544.
[15] Hatfield, J. L., Prueger, J. H. (2010): Value of using different vegetative indices to quantify agricultural crop characteristics at different growth stages under varying management practices. – Remote Sensing 2: 562-578.
[16] Idso, S., Jackson, R., Pinter Jr, P., Reginato, R., Hatfield, J. (1981): Normalizing the stress-degree-day parameter for environmental variability. – Agricultural Meteorology 24: 45-55.
[17] Jackson, R. D., Idso, S., Reginato, R., Pinter Jr, P. (1981): Canopy temperature as a crop water stress indicator. – Water Resources Research 17: 1133-1138.
[18] Jiang, Z.-Y., Li, X.-Y., Ma, Y.-J. (2013): Water and energy conservation of rainwater harvesting system in the Loess Plateau of China. – Journal of Integrative Agriculture 12: 1389-1395.

http://www.aloki.hu ● ISSN 1589 1623 (Print) ● ISSN 1785 0037 (Online)
DOI: http://dx.doi.org/10.15666/aeer/1803_40874102

[19] Jin, N., Ren, W., Tao, B., He, L., Ren, Q., Li, S., Yu, Q. (2018): Effects of water stress on water use efficiency of irrigated and rainfed wheat in the Loess Plateau, China. – Science of the Total Environment 642: 1-11.
[20] Jones, H. G. (1999): Use of infrared thermometry for estimation of stomatal conductance as a possible aid to irrigation scheduling. – Agricultural and Forest Meteorology 95: 139-149.
[21] Jones, H. G. (2013): Plants and Microclimate: A Quantitative Approach to Environmental Plant Physiology. – Cambridge University Press, Cambridge.
[22] Jones, H. G., Stoll, M., Santos, T., Sousa, C. D., Chaves, M. M., Grant, O. M. (2002): Use of infrared thermography for monitoring stomatal closure in the field: application to grapevine. – Journal of Experimental Botany 53: 2249-2260.
[23] Jordan, C. F. (1969): Derivation of leaf-area index from quality of light on the forest floor. – Ecology 50: 663-666.
[24] Khanal, S., Fulton, J., Shearer, S. (2017): An overview of current and potential applications of thermal remote sensing in precision agriculture. – Computers and Electronics In Agriculture 139: 22-32.
[25] Khorsandi, A., Hemmat, A., Mireei, S. A., Amirfattahi, R., Ehsanzadeh, P. (2018): Plant temperature-based indices using infrared thermography for detecting water status in sesame under greenhouse conditions. – Agricultural Water Management 204: 222-233.
[26] Maini, R., Aggarwal, H. (2008): Study and comparison of various image edge detection techniques. – International Journal of Image Processing (IJIP) 3(1).
[27] Meron, M., Tsipris, J., Orlov, V., Alchanatis, V., Cohen, Y. (2010): Crop water stress mapping for site-specific irrigation by thermal imagery and artificial reference surfaces. – Precision Agriculture 11: 148-162.
[28] Möller, M., Alchanatis, V., Cohen, Y., Meron, M., Tsipris, J., Naor, A., Ostrovsky, V., Sprintsin, M., Cohen, S. (2006): Use of thermal and visible imagery for estimating crop water status of irrigated grapevine. – Journal of Experimental Botany 58: 827-838.
[29] Pallavi, S., Mallapur, J. D., Bendigeri, K. Y. (2017): Remote sensing and controlling of greenhouse agriculture parameters based on IOT. – International Conference on Big Data, IOT and Data Science (BID), 2017, IEEE, 44-48.
[30] Poblete-Echeverr A, C., Sepulveda-Reyes, D., Ortega-Farias, S., Zu Iga, M., Fuentes, S. (2014): Plant water stress detection based on aerial and terrestrial infrared thermography: a study case from vineyard and olive orchard. – XXIX International Horticultural Congress on Horticulture: Sustaining Lives, Livelihoods and Landscapes (IHC2014) 1112: 141-146.
[31] Prasad, S., Bruce, L. M. (2011): A Divide-and-Conquer Paradigm for Hyperspectral Classification and Target Recognition. – In: Prasad, S. et al. (eds.) Optical Remote Sensing. Springer, Berlin.
[32] Quattrochi, D. A., Luvall, J. C. (1999): Thermal infrared remote sensing for analysis of landscape ecological processes: methods and applications. – Landscape Ecology 14: 577-598.
[33] Rud, R., Cohen, Y., Alchanatis, V., Levi, A., Brikman, R., Shenderey, C., Heuer, B., Markovitch, T., Dar, Z., Rosen, C. (2014): Crop water stress index derived from multi-year ground and aerial thermal images as an indicator of potato water status. – Precision Agriculture 15: 273-289.
[34] Stark, B., Smith, B., Chen, Y. (2014): Survey of thermal infrared remote sensing for unmanned aerial systems. – International Conference on Unmanned Aircraft Systems (ICUAS), 2014, IEEE 1294-1299.
[35] Tanner, C. (1963): Plant temperatures 1. – Agronomy Journal 55: 210-211.
[36] Testi, L., Goldhamer, D., Iniesta, F., Salinas, M. (2008): Crop water stress index is a sensitive water stress indicator in pistachio trees. – Irrigation Science 26: 395-405.

http://www.aloki.hu ● ISSN 1589 1623 (Print) ● ISSN 1785 0037 (Online)
DOI: http://dx.doi.org/10.15666/aeer/1803_40874102